Interturn short circuit modelling in dual three-phase PMSM

KOZOVSKÝ, M.; BUCHTA, L.; BLAHA, P.

IECON 2022 – 48th Annual Conference of the IEEE Industrial Electronics Society

ISBN: 10.1109/IECON49645.2022.9968364

DOI: https://doi.org/10.1109/IECON49645.2022.9968364

Accepted manuscript

Interturn short circuit modelling in dual three-phase PMSM

1st Matus Kozovsky
CEITEC
Brno University of Technology
Brno, Czech Republic
https://orcid.org/0000-0002-1547-1003

2nd Ludek Buchta
CEITEC
Brno University of Technology
Brno, Czech Republic
https://orcid.org/0000-0002-8954-3495

3rd Petr Blaha
CEITEC
Brno University of Technology
Brno, Czech Republic
https://orcid.org/0000-0001-5534-2065

***Abstract*—In this study, model of a multi-phase permanent magnet synchronous motor is demonstrated. The model is designed to allow simulations of inter-turn short circuit faults of various severity. The considered multi-phase motor is connected as a dual three-phase system. In this case, stator windings are divided into two electrically separated sub-systems. Nevertheless, the magnetic coupling between sub-systems needs to be taken into account in general. The motor model is designed to take into account the exact stator coils distribution. In this case motor uses combination of serial and parallel connections. Model is implemented in MATLAB/Simulink using SimScape environment. The paper also shows a comparison of the behavior of a real PMS motor and derived model behavior.**

***Index Terms*—Multi-phase motor model, interturn short-circuit, PMSM, fault model**

I. Introduction

Nowadays, permanent magnet synchronous motors (PMSM) are typically used due to their high power-to-weight ratio and excellent efficiency. PMS motors are thus often used in industry, automotive, or aviation. One of the requirements is to achieve sufficient motor power at a wide range of speeds. This requirement is typical, for instance, in electric vehicle powertrains. Similar needs also arrise in aviation applications [1]. The possibility to run the motor in a field weakening mode is often required for this reason.

Besides advantages, PMSM also has a couple of disadvantages. The rotating rotor always generates a back-EMF voltage into stator windings. The generated voltage can be higher than DC-link voltage if the motor is designed to operate in the field weakening mode. This feature can be very problematic during the motor or power inverter fault. Closely related problem of PMSM are internal short-circuit faults. These faults are caused by insulation material degradation induced by machine vibrations and high voltage and temperature stress. The loss of the insulation dielectric properties between the two conductors causes the formation of a closed-loop inside the stator winding. The formed closed-loop is magnetically coupled to other healthy windings and rotor magnets. Closed-loop electrical properties and induced voltage generated by spinning rotor result in the fault current flowing through this loop. The amplitude of a fault current can be many times higher than the nominal motor current. The fault current can subsequently result in temperature rise up and further emergence of new interturn short-circuits. Thus, this kind of fault should be detected as soon as possible.

In recent years, many publications have dealt with the problem of modeling motors under electrical or mechanical fault. The models can be beneficial for fault detection algorithms [2]. Most studies present motor winding as one coil with mutual inductances only to other phase windings. Model created using such a simplified method does not ideally reflect the real motor behavior, which can be substantially different. This simplified approach can be effectively used for motors with non-concentric windings, as Mazzoletti et al. [3] demonstrate. On the other hand, Zhao et al. [1] demonstrate the significant influence of the asymmetric windings and magnetic circuit on the resulting behavior of the motor. The importance of detailed winding analysis is evident for motors with concentric windings. Behavioral differences between the model and real motor are more significant in high-speed operation. Simulated fault current can be higher than real fault current because of the simplification, especially in motors with many serially connected concentric coils. The motor model must take into account the internal wiring structure of the motor to achieve the required accuracy in simulating inter-turn short circuit fault behavior [4].

All mentioned modeling strategies consider three-phase systems. This study describes the analysis of a dual three-phase machine. Multi-phase structures in various configurations can be used to achieve fail-operation behavior [5]. In this case, a precise multi-phase model with the possibility to simulate an interturn short-circuit is essential. This study considers a dual three-phase PMS motor with interlaced sub-systems and concentric stator coils. This structure is fully symmetrical and does not require special modifications of the control algorithm.

The work has been performed in the project AI4DI: Artificial Intelligence for Digitizing Industry, under grant agreement No 826060/8A19001. The work was co-funded by grants of Ministry of Education, Youth and Sports of the Czech Republic and Electronic Component Systems for European Leadership Joint Undertaking (ECSEL JU). The work was supported by the infrastructure of RICAIP that has received funding from the European Union's Horizon 2020 research and innovation programme under grant agreement No 857306 and from Ministry of Education, Youth and Sports under OP RDE grant agreement No CZ.02.1.01/0.0/0.0/17_043/0010085

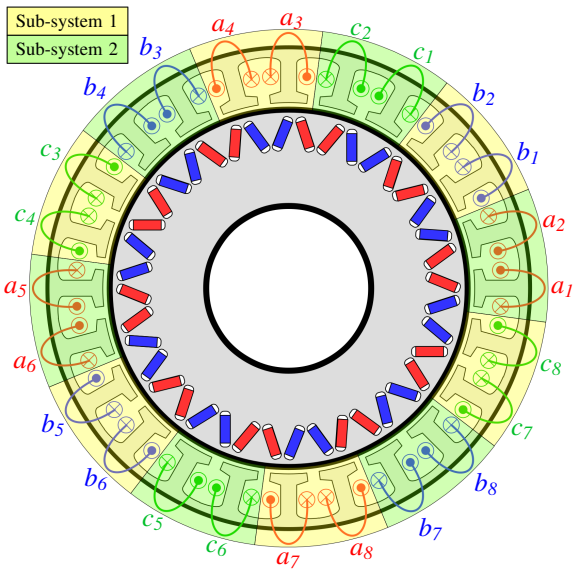

Fig. 1. The experimental motor structure and assignment of individual coils into sub-systems

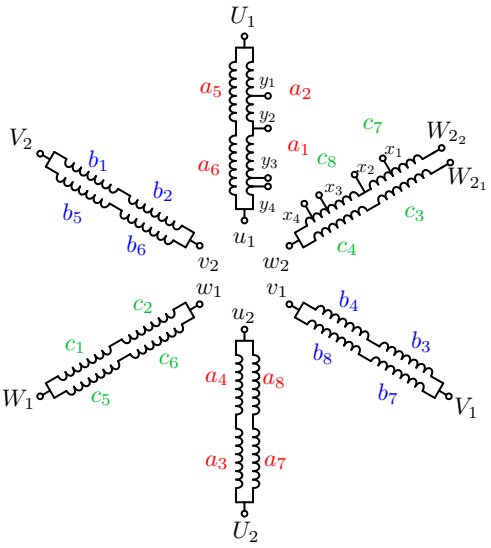

Fig. 2. The experimental motor winding arrangement, winding taps y_{1-4} and x_{1-4} can be used to emulate interturn short-circuit fault

II. Experimental Motor Description

The derived mathematical model must respect the structure of the experimental motor. An essential requirement for fail-operational capability is that the motor can operate under an active short circuit in case of failure. This brings together requirement on following properties. The field weakening index of the machine is lower than one which insures that the machine (subsystem) can be completely field weakened to suppress the faulty current. The next property is low mutual inductance between sub-systems. Low mutual inductance between sub-systems allows isolating the fault in one sub-system while the second sub-system can continue in operation. A properly designed coil arrangement can give low mutual inductances. This statement can also be seen from the calculations derived in the following part of the paper.

The experimental motor has 24 stator slots and ten pole pairs in the rotor. The stator contains 24 concentric coils. The coil arrangement inside the motor is shown in Fig. 1. According to the diagram shown in Fig. 2, individual coils are connected in a serial and parallel way to form two sets of three-phase windings. Parameters of the custom made experimental machine are shown in the table I. The motor was designed to emulate various stator winding faults with selectable severity. The mutual interconnection of winding taps $y_1 - y_4$ can be used to emulate interturn short-circuit faults in phase U. The same fault can be emulated in phase W using taps $x_1 - x_4$. It is apparent that the taps and windings ends can also be used to emulate phase to phase short-circuit fault in one sub-system or even short-circuits between sub-systems depending on the used motor configuration.

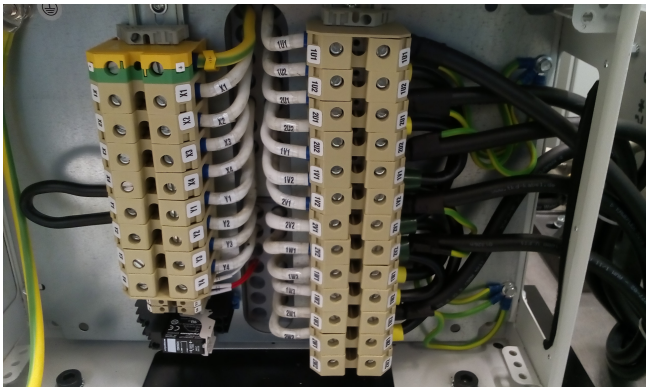

Fig. 3. The experimental motor terminal box

TABLE I
Experimental Motor Parameters

Name	Symbol	Value	Unit
DC voltage	U_{DC}	200	V
Maximum continues motor current	I_s	107	A
Winding resistance	R_s	6.5	mΩ
Back-EMF constant	ψ_m	0.0117	Vs/rad
Winding inductance	L_{u-v}	180	µH
Nominal speed	ω_n	8000	rpm
Maximum speed	ω_M	10500	rpm
Nominal power	P_c	30160	W
Number of pole pairs	Pp	10	-
Characteristic current	I_{ch}	81	A

III. Dual Three-Phase PMSM Model

The motor model is based on the magnetic flux linkages analysis between individual stator coils. Each coil has its self-inductance and also magnetic linkage to other coils. Magnetic coupling factor is denoted by variables γ_d where d represents the distance between stator slots or distance between individual coils. The path of magnetic flux can be seen in Fig. 4. Considering only the coils without assigning them to the

subsystems $(a_1, a_2, ..., c_7, c_8)$, flux linkage λ_{a1} of first coil is given by (1) where S denotes the number of motor slots. Variables L_{sm} and L_{sl} denote the single-coil self and leakage inductance. Similar equations can be derived for the other 23 coils. Individual signs in (1) need to reflect coil orientation.

$$\begin{aligned}\lambda_{a_1} = (L_{sm} + L_{sl})i_{a_1} + (&\gamma_1 i_{a_2} + \gamma_2 i_{b_1} - \gamma_3 i_{b_2} - \gamma_4 i_{c_1} \\ &+\gamma_5 i_{c_2} + \gamma_6 i_{a_3} - \gamma_7 i_{a_4} - \gamma_8 i_{b_3} + \gamma_9 i_{b_4} + \gamma_{10} i_{c_3} \\ &-\gamma_{11} i_{c_4} - \gamma_{12} i_{a_5} + \gamma_{11} i_{a_6} + \gamma_{10} i_{b_5} - \gamma_9 i_{b_6} - \gamma_8 i_{c_5} \\ &+\gamma_7 i_{c_6} + \gamma_6 i_{a_7} - \gamma_5 i_{a_8} - \gamma_4 i_{b_7} + \gamma_3 i_{b_8} + \gamma_2 i_{c_7} \\ &-\gamma_1 i_{c_8}) * \frac{L_{sm}}{S-1} \end{aligned} \tag{1}$$

Magnetic flux equations can be simplified considering the serial connection of adjacent coils of the same phase. In this case, the magnetic flux of serial connection of two coils is denoted by variable $\lambda_{a_{ij}}$. (1) can be rewritten into (2).

$$\begin{aligned}\lambda_{a_{12}} = \lambda_{a_1} + \lambda_{a_2} = (&2L_{sm} + 2L_{sl} + 2\gamma_1 \frac{L_{sm}}{S-1}) i_{a_{12}} \\ &+(\sigma_1 i_{b_{12}} + \sigma_2 i_{c_{12}} + \sigma_3 i_{a_{34}} + \sigma_4 i_{b_{34}} + \sigma_5 i_{c_{34}} \\ &+(2\gamma_{11} - 2\gamma_{12}) i_{a_{56}} + \sigma_5 i_{b_{56}} + \sigma_4 i_{c_{56}} + \sigma_3 i_{a_{78}} \\ &+\sigma_2 i_{b_{78}} + \sigma_1 i_{c_{78}}) * \frac{L_{sm}}{S-1} \end{aligned} \tag{2}$$

where $\sigma_1 = 2\gamma_2 - \gamma_1 - \gamma_3$, $\sigma_2 = \gamma_3 + \gamma_5 - 2\gamma_4$

$\sigma_3 = 2\gamma_6 - \gamma_5 - \gamma_7$, $\sigma_4 = \gamma_7 + \gamma_9 - 2\gamma_8$

$\sigma_5 = 2\gamma_{10} - \gamma_9 - \gamma_{11}$

In this case, following condition (3) is met for all currents in (2).

$$i_{x_n} = i_{x_m} = i_{x_{nm}} \tag{3}$$

Considering the same current flowing through parallel paths, we can calculate the magnetic flux generated by the whole phase winding (4).

$$\begin{aligned}\lambda_{u_1} = \lambda_{a_{12}} + \lambda_{a_{45}} = \\ (2L_{sm} + 2L_{sl} + (2\gamma_1 + 2\gamma_{11} - 2\gamma_{12}) \frac{L_{sm}}{S-1}) \frac{i_{u_1}}{2} \\ +(\delta_1 \frac{i_{v_1} + i_{w_1}}{2} + \delta_2 \frac{i_{u_2}}{2} + \delta_3 \frac{i_{v_2} + i_{w_2}}{2}) \frac{L_{sm}}{S-1} \end{aligned} \tag{4}$$

where $\delta_1 = \gamma_3 + \gamma_5 - 2\gamma_4 + \gamma_7 + \gamma_9 - 2\gamma_8$

$\delta_2 = 4\gamma_6 - 2\gamma_5 - 2\gamma_7$

$\delta_3 = 2\gamma_2 - \gamma_1 - \gamma_3 + 2\gamma_{10} - \gamma_9 - \gamma_{11}$

The electrical part of PMSM can be described by equation (5). In this case, we speak about the model of healthy motor.

$$\boldsymbol{u}_{uvw_{12}} = \boldsymbol{R}_{uvw_{12}} \boldsymbol{i}_{uvw_{12}} + \frac{\mathrm{d}\boldsymbol{L}_{uvw_{12}} \boldsymbol{i}_{uvw_{12}}}{\mathrm{d}t} + \boldsymbol{e}_{uvw_{12}} \tag{5}$$

where $\boldsymbol{u}_{uvw_{12}} = [u_{u_1}, u_{v_1}, u_{w_1}, u_{u_2}, u_{v_2}, u_{w_2}]^\top$

$\boldsymbol{i}_{uvw_{12}} = [i_{u_1}, i_{v_1}, i_{w_1}, i_{u_2}, i_{v_2}, i_{w_2}]^\top$

Variables $\boldsymbol{v}_{uvw_{12}}$ and $\boldsymbol{i}_{uvw_{12}}$ denote motor voltages and currents, respectively.

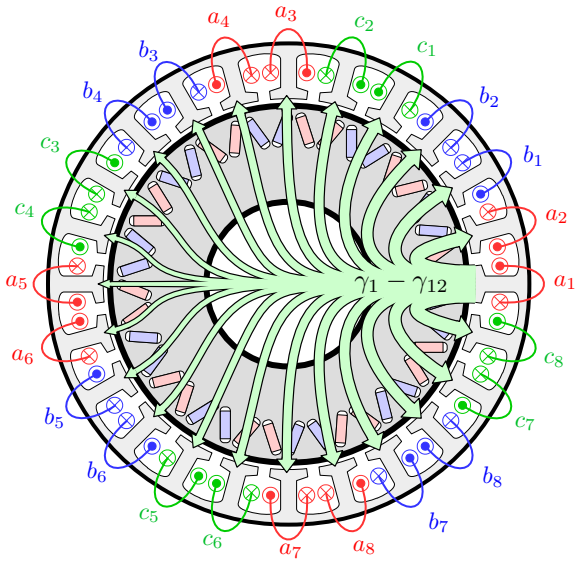

Fig. 4. Visualisation of the magnetic flux flow generated by the a_1 winding

$$\boldsymbol{R}_{uvw_{12}} = \begin{bmatrix} R_s & 0 & 0 & 0 & 0 & 0 \\ 0 & R_s & 0 & 0 & 0 & 0 \\ 0 & 0 & R_s & 0 & 0 & 0 \\ 0 & 0 & 0 & R_s & 0 & 0 \\ 0 & 0 & 0 & 0 & R_s & 0 \\ 0 & 0 & 0 & 0 & 0 & R_s \end{bmatrix} \tag{6}$$

$$\boldsymbol{L}_{uvw_{12}} = \begin{bmatrix} L_{aa} & L_{ab} & L_{ac} & L_{m_{aa}} & L_{m_{ab}} & L_{m_{ac}} \\ L_{ab} & L_{bb} & L_{bc} & L_{m_{ab}} & L_{m_{bb}} & L_{m_{bc}} \\ L_{ac} & L_{bc} & L_{cc} & L_{m_{ac}} & L_{m_{bc}} & L_{m_{cc}} \\ L_{m_{aa}} & L_{m_{ab}} & L_{m_{ac}} & L_{aa} & L_{ab} & L_{ac} \\ L_{m_{ab}} & L_{m_{bb}} & L_{m_{bc}} & L_{ab} & L_{bb} & L_{bc} \\ L_{m_{ac}} & L_{m_{bc}} & L_{m_{cc}} & L_{ac} & L_{bc} & L_{cc} \end{bmatrix} \tag{7}$$

where $L_{aa} = L_{bb} = L_{cc} = L_{sm} + L_{sl} + (\gamma_1 + \gamma_{11} - \gamma_{12}) \frac{L_{sm}}{S-1}$

$L_{ab} = L_{ac} = L_{bc} = \frac{\gamma_3 + \gamma_5 - 2\gamma_4 + \gamma_7 + \gamma_9 - 2\gamma_8}{2}$

$L_{m_{aa}} = L_{m_{bb}} = L_{m_{cc}} = 2\gamma_6 - \gamma_5 - \gamma_7$

$L_{m_{ab}} = L_{m_{ac}} = L_{m_{bc}} = \frac{2\gamma_2 - \gamma_1 - \gamma_3 + 2\gamma_{10} - \gamma_9 - \gamma_{11}}{2}$

$$\boldsymbol{e}_{uvw_{12}} = \omega_e \psi_m \begin{bmatrix} \cos(\theta) \\ \cos(\theta + \frac{2\pi}{3}) \\ \cos(\theta - \frac{2\pi}{3}) \\ \cos(\theta) \\ \cos(\theta + \frac{2\pi}{3}) \\ \cos(\theta - \frac{2\pi}{3}) \end{bmatrix} \tag{8}$$

Variables $\boldsymbol{R}_{uvw_{12}}$ and $\boldsymbol{L}_{uvw_{12}}$ denote the matrix of resistances and the inductance matrix. Back-EMF voltage generated by the motor rotation is given by $\boldsymbol{e}_{uvw_{12}}$. θ denotes electrical angle between the quadrature axis of rotor magnets and the phase u_1. Variables ω_e and ψ_m represent actual electrical motor speed and rotor permanent magnet flux.

Another critical part of the motor model is how motor currents or magnetic flux is converted into mechanical torque. Motor torque can be calculated in stator or rotor coordinates. Mechanical torque generated by the motor in stator coordinates can be calculated using (9).

$$T_e = Pp\left(\frac{1}{2}\boldsymbol{i}_{uvw_{12}}{}^{\top}+\frac{\mathrm{d}\boldsymbol{L}_{uvw_{12}}}{\mathrm{d}\theta}\boldsymbol{i}_{uvw_{12}}+\frac{\boldsymbol{i}_{uvw_{12}}{}^{\top}\boldsymbol{e}_{uvw_{12}}}{\omega_e}\right) \quad (9)$$

The relationship between the rotor position θ, electrical speed ω_e and mechanical speed ω_m is given by (10) and (11) .

$$\frac{\mathrm{d}\theta}{\mathrm{d}t} = \omega_e = \omega_m \cdot Pp \quad (10)$$

$$\frac{\mathrm{d}\omega_e}{\mathrm{d}t} = \frac{1}{J}\left(Pp(T_e - T_l) - B\omega_e\right) \quad (11)$$

Variable T_l represents loads torque. Variables J and B denote mechanical system inertia and viscous friction coefficient.

IV. Model Extension for Fault Simulation

The model described in previous section can simulate dual three-phase motor behavior in healthy conditions; however, additional modifications are needed to enable the interturn short circuit fault simulation. The fault is modelled in phase U of the first sub-system, specifically in coil a_1. The current through parallel paths of the winding will no longer be the same. For this reason, serial connection of coils will be simulated separately with currents i_{a12} and i_{a56}. Various depths of the interturn short-circuit fault are given by the parameter ϑ, which is defined as the ratio of short-circuited turns to a total number of turns per coil. Mutual inductance between short-circuited part and the rest of the coil is close to one. In this case, the self-inductance of the short-circuited part L_f and the rest of the coil L^*_{a1} is given by (12) and (13).

$$L_f = \vartheta^2(L_{sm} + L_{sl}) \quad (12)$$

$$L^*_{a1} = (1-\vartheta)^2(L_{sm} + L_{sl}) \quad (13)$$

Mutual inductance between the short-circuited part and the rest of the healthy coil is given by (14).

$$L_{fa1} = (1-\vartheta)\vartheta(L_{sm} + L_{sl}) \quad (14)$$

The equation (5) can be used for faulty model, however it needs to be extended into (15). The phase current i_{u_1} is split into $i_{a_{12}}$ and $i_{a_{56}}$.

$$\boldsymbol{u}_{uvw_{12f}} = \boldsymbol{R}_{uvw_{12f}}\boldsymbol{i}_{uvw_{12f}} + \frac{\mathrm{d}\boldsymbol{L}_{uvw_{12f}}\boldsymbol{i}_{uvw_{12f}}}{\mathrm{d}t} + \boldsymbol{e}_{uvw_{12f}} \quad (15)$$

where $\boldsymbol{u}_{uvw_{12f}} = [u_{u_1}-u_f, u_{u_1}, u_f, u_{v_1}, u_{w_1}, u_{u_2}, u_{v_2}, u_{w_2}]^{\top}$

$\boldsymbol{i}_{uvw_{12f}} = [i_{a_{12}}, i_{a_{56}}, i_f, i_{v_1}, i_{w_1}, i_{u_2}, i_{v_2}, i_{w_2}]^{\top}$

The voltage on the interturn short-circuits part is given by u_f during the fault. This voltage is zero during the fault. New matrixes for fault simulation are given by (16) and (17). Some internal parts of inductance matrix shown in (17) are the same as (7). The back-EMF voltage for modified model is given by (18). The equation needs to reflect phase shift φ between two serial coils a_1 and a_2. φ for presented structure is 30 electrical

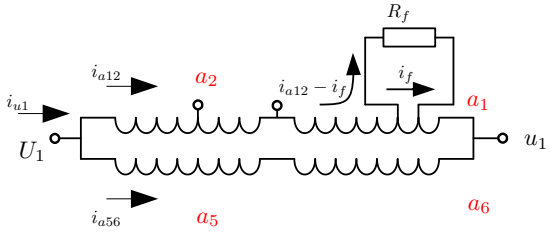

Fig. 5. Phase u_1 detail with interturn short-circuit fault

degrees. Coil orientation needs to be considered. This feature represents significant difference between simplified and full model. The torque generated by machine can be calculated using modified version of (9).

$$\boldsymbol{R}_{uvw_{12f}} = \begin{bmatrix} 2R_s{-}\vartheta R_s & 0 & 0 & 0 & 0 & 0 & 0 & 0 \\ 0 & 2Rs & 0 & 0 & 0 & 0 & 0 & 0 \\ 0 & 0 & \vartheta R_s & 0 & 0 & 0 & 0 & 0 \\ 0 & 0 & 0 & R_s & 0 & 0 & 0 & 0 \\ 0 & 0 & 0 & 0 & R_s & 0 & 0 & 0 \\ 0 & 0 & 0 & 0 & 0 & R_s & 0 & 0 \\ 0 & 0 & 0 & 0 & 0 & 0 & R_s & 0 \\ 0 & 0 & 0 & 0 & 0 & 0 & 0 & R_s \end{bmatrix} \quad (16)$$

$$\boldsymbol{L}_{uvw_{12f}} = \begin{bmatrix} L_{af} & L_{afh} & L_{aff} & L_{afb} & L_{afc} & L_{m_{afa}} & L_{m_{afb}} & L_{m_{afc}} \\ L_{afh} & L_{ah} & L_{ahf} & L_{ab} & L_{ac} & L_{m_{aa}} & L_{m_{ab}} & L_{m_{ac}} \\ L_{aff} & L_{ahf} & L_f & L_{fb} & L_{fc} & L_{mfa} & L_{mfb} & L_{mfc} \\ L_{afb} & L_{ab} & L_{fb} & L_{bb} & L_{bc} & L_{m_{ab}} & L_{m_{bb}} & L_{m_{bc}} \\ L_{afc} & L_{ac} & L_{fc} & L_{bc} & L_{cc} & L_{m_{ac}} & L_{m_{bc}} & L_{m_{cc}} \\ L_{m_{afa}} & L_{m_{aa}} & L_{mfa} & L_{m_{ab}} & L_{m_{ac}} & L_{aa} & L_{ab} & L_{ac} \\ L_{m_{afb}} & L_{m_{ab}} & L_{mfb} & L_{m_{bb}} & L_{m_{bc}} & L_{ab} & L_{bb} & L_{bc} \\ L_{m_{afc}} & L_{m_{ac}} & L_{mfc} & L_{m_{bc}} & L_{m_{cc}} & L_{ac} & L_{bc} & L_{cc} \end{bmatrix} \quad (17)$$

where

$$\begin{aligned} L_{ah} &= 2L_{sm}{+}2L_{sl}{+}2\gamma_1 L_{sm}/(S{-}1) \\ L_{af} &= (L_{sm}{+}L_{sl})(1{+}(1{-}\vartheta)^2){+}(1{-}\vartheta)2\gamma_1 L_{sm}/(S{-}1) \\ L_f &= \vartheta^2(L_{sm}{+}L_{sl}) \\ L_{aff} &= (\vartheta{-}\vartheta^2)(L_{sm}{+}L_{sl}) + \vartheta\gamma_1 L_{sm}/(S{-}1) \\ L_{afh} &= (1{-}\vartheta/2)(\gamma_{11}{-}\gamma_{12})L_{sm}/(S{-}1) \\ L_{ahf} &= \vartheta/2(\gamma_{11}{-}\gamma_{12})L_{sm}/(S{-}1) \\ L_{afb} &\approx (1{-}\vartheta/2)L_{ab}, \qquad L_{fb} \approx \vartheta/2 L_{ab} \\ L_{afc} &\approx (1{-}\vartheta/2)L_{ac}, \qquad L_{fc} \approx \vartheta/2 L_{ac} \\ L_{m_{afa}} &\approx (1{-}\vartheta/2)L_{m_{aa}}, \quad L_{m_{fa}} \approx \vartheta/2 L_{m_{aa}} \\ L_{m_{afb}} &\approx (1{-}\vartheta/2)L_{m_{ab}}, \quad L_{m_{fb}} \approx \vartheta/2 L_{m_{ab}} \\ L_{m_{afc}} &\approx (1{-}\vartheta/2)L_{m_{ac}}, \quad L_{m_{fc}} \approx \vartheta/2 L_{m_{ac}} \end{aligned}$$

$$\boldsymbol{e}_{uvw_{12f}} = \omega_e\psi_m \begin{bmatrix} \frac{0.5}{\cos(\varphi)}\left(\cos(\theta{+}\frac{\varphi}{2}){+}\cos(\theta{-}\frac{\varphi}{2})(1{-}\frac{\vartheta}{2})\right) \\ \cos(\theta) \\ \frac{\vartheta}{2}\cos(\theta-\varphi) \\ \cos(\theta+\frac{2\pi}{3}) \\ \cos(\theta-\frac{2\pi}{3}) \\ \cos(\theta) \\ \cos(\theta+\frac{2\pi}{3}) \\ \cos(\theta-\frac{2\pi}{3}) \end{bmatrix} \quad (18)$$

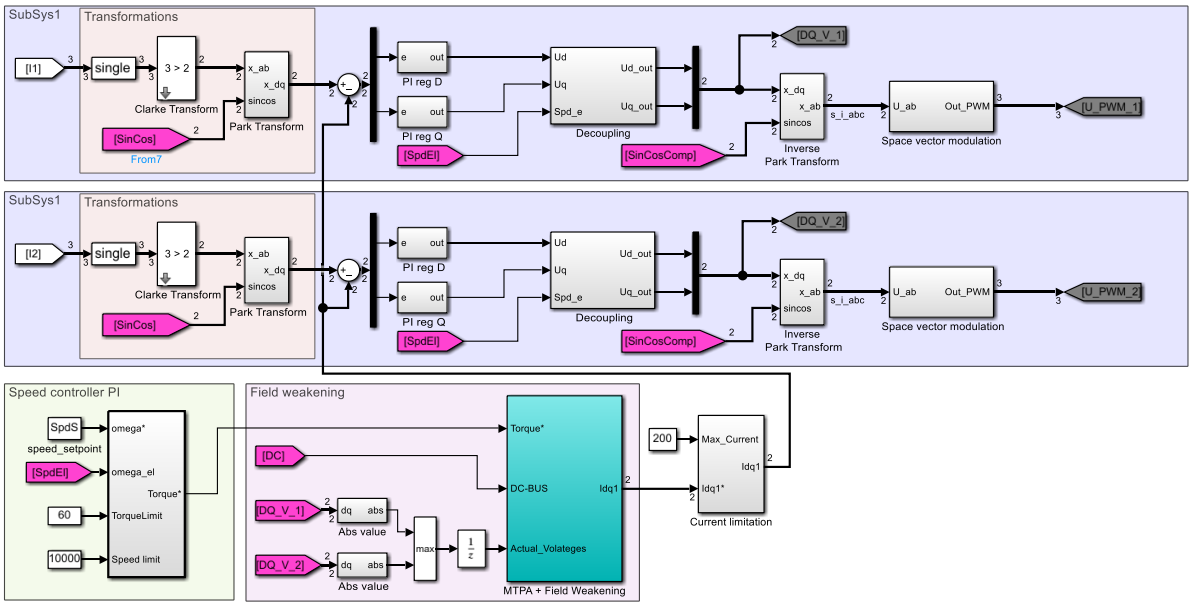

Fig. 6. Implemented control algorithm (Speed controller + MTPA + Field Weakening + Current controllers + Decoupling)

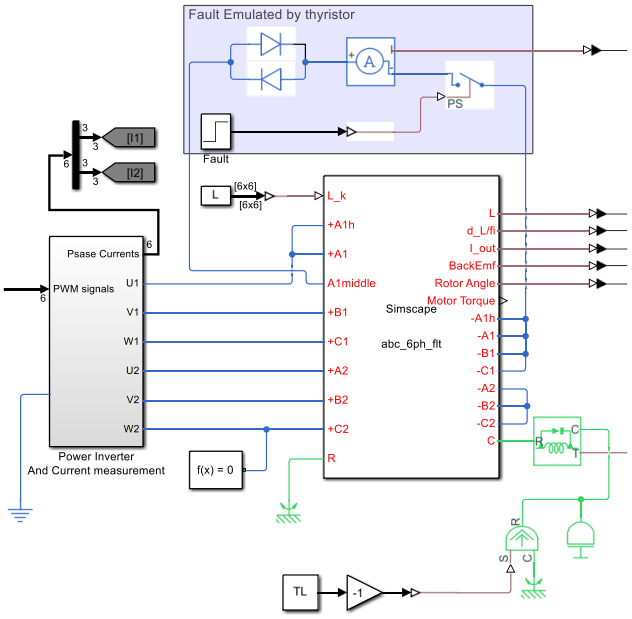

Fig. 7. Implemented PMSM model in MATLAB/Simulink using Simscape

V. Comparisons with real PMS motor

This chapter shows a comparison of measured and simulated motor currents during the occurrence of an interturn short-circuit on the winding. Mutual inductances between the formed inner loop and other windings were measured using the RLC meter. Another option would be using FEM simulations or calculating the equivalent magnetic circuit to determine individual $\gamma_1 - \gamma_{12}$ coefficients. It is possible to consider the coefficients as a function of rotor position to improve the conformity of the model with reality.

A field-oriented control algorithm was implemented in a dual three-phase power inverter for the motor control. The same algorithm was also used in simulations. The used control algorithm can be seen in Fig. 6. The decoupling used in control algorithm which allows operating the motor in high speed is derived based on [6].

The motor model is implemented in MATLAB/Simulink using a custom Simscape blocks. Simscape allows an acausal modeling approach. Coil A1 is divided into A1h and A1 parts. The point A1 in the middle represents prepared winding tap. Short-circuit fault is generated using thyristors for short reaction time and measurement repeatability during the real experiments. Fig. 9 shows an experimental motor connected to a dynamometer and the power inverter. The motor was running at 4270 rpm with a load of 10 Nm. The relay contacts prove to be problematic as the resistance changes between repeated switching. For this reason, a thyristor is used to form an interturn short-circuit. This fact is taken into account by the addition of anti-parallel diodes into the model. The motor model is shown in Fig. 7.

Fig. 8 and Fig. 10 show the current of the measured and simulated behavior. For the comparison, the operating point was selected to show the model's compliance even in the high-speed region. At lower speeds, it is possible to observe differences due to nonlinearities such as deadtime.

VI. Conclusion

The first part of the paper described modeling methods and their limitations depending on the motor winding arrangement. The advantages of multi-phase motors are also presented.

Second part presents the model of a dual three-phase PMS motor with a combination of serial and parallel connected windings and interlaced sub-systems. The presented model

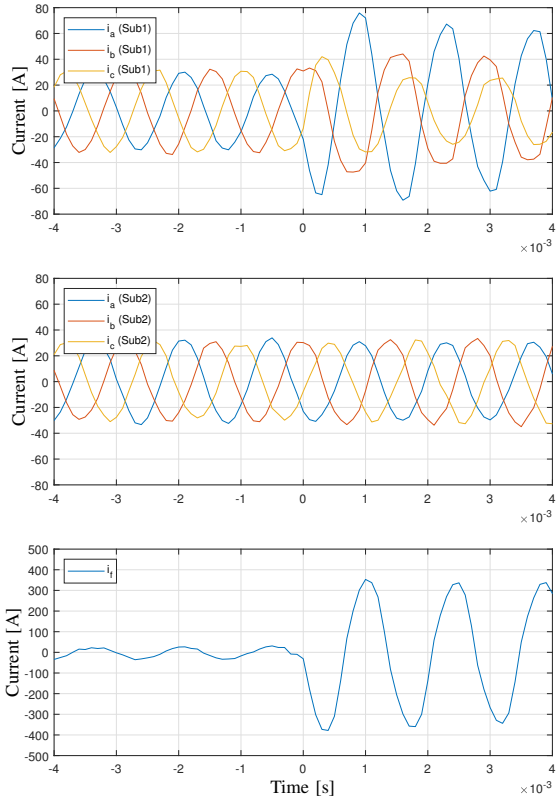

Fig. 8. Measured motor currents on real PMSM (4270 rpm 10 Nm load)

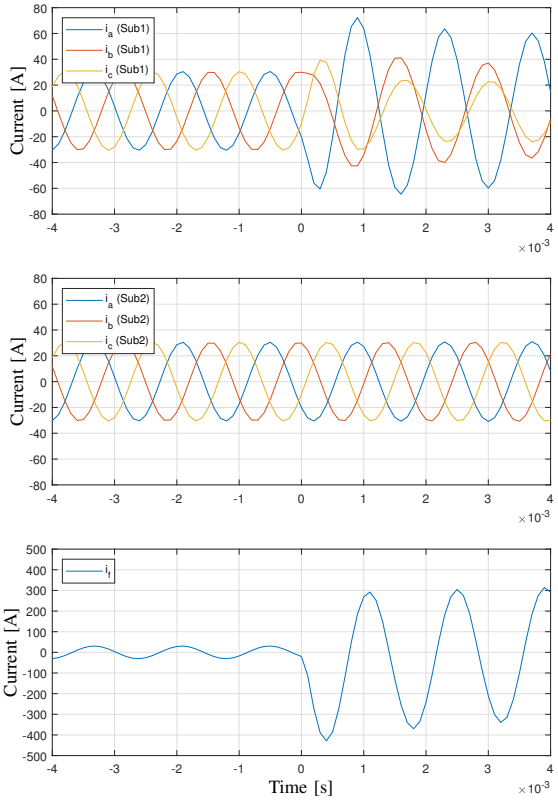

Fig. 10. Simulated motor currents using derived model (4270 rpm 10 Nm load)

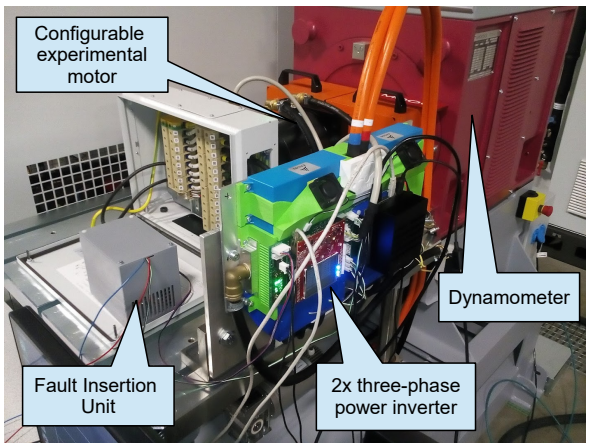

Fig. 9. Dynamometer and experimental PMSM under test

was extended to allow interturn short-circuit fault emulation. The fault can be emulated in one coil. The real motor uses concentric stator windings.

The last part presents the testbench used for real motor measurement and model implementation into the SimScape environment of MATLAB/Simulink. Figures from measurements and simulations show conformity between the presented model and the real PMS motor.

REFERENCES

[1] T. Zhao, S. Wu, and S. Cui, "Multiphase PMSM With Asymmetric Windings for More Electric Aircraft," *IEEE Transactions on Transportation Electrification*, vol. 6, no. 4, pp. 1592–1602, dec 2020. [Online]. Available: https://ieeexplore.ieee.org/document/9099484/

[2] L. Bao, G. Yao, S. Chen, Z. Wang, X. Hu, and Y. Huang, "An On-line Detection Method for Single-Phase Inter-Turn Fault Occurring in High-Speed PMSM," in *2020 23rd International Conference on Electrical Machines and Systems (ICEMS)*. IEEE, nov 2020, pp. 1095–1100. [Online]. Available: https://ieeexplore.ieee.org/document/9290898/

[3] M. A. Mazzoletti, G. R. Bossio, C. H. De Angelo, and D. R. Espinoza-Trejo, "A Model-Based Strategy for Interturn Short-Circuit Fault Diagnosis in PMSM," *IEEE Transactions on Industrial Electronics*, vol. 64, no. 9, pp. 7218–7228, sep 2017. [Online]. Available: http://ieeexplore.ieee.org/document/7889000/

[4] B.-G. Gu, J.-H. Choi, and I.-S. Jung, "Development and Analysis of Interturn Short Fault Model of PMSMs With Series and Parallel Winding Connections," *IEEE Transactions on Power Electronics*, vol. 29, no. 4, pp. 2016–2026, apr 2014. [Online]. Available: http://ieeexplore.ieee.org/document/6522484/

[5] M. Kozovsky, L. Buchta, and P. Blaha, "Compensation methods of interturn short-circuit faults in dual three-phase PMSM," in *IECON 2020 The 46th Annual Conference of the IEEE Industrial Electronics Society*. IEEE, oct 2020, pp. 4833–4838. [Online]. Available: https://ieeexplore.ieee.org/document/9254734/

[6] G. Xingye, L. Chuang, Z. Yuefei, and W. Kai, "Analysis and dynamic decoupling control schemes for PMSM current Loop," in *2016 IEEE International Conference on Aircraft Utility Systems (AUS)*. IEEE, 2016, pp. 570–574. [Online]. Available: http://ieeexplore.ieee.org/document/7748115/